ERDC MSRC/PET TR/00-16

A Comparison of the SWAN and WAM Wave Models for Nearshore Wave Predictions

by

Stephen Wornom
David J. S. Welsh

18 April 2000

06h0052000

A Comparison of the SWAN and WAM Wave Models for Nearshore Wave Predictions

Stephen Wornom*
Department of Civil and Environmental Engineering
and Geodetic Science
The Ohio State University

David J. S. Welsh†
Department of Civil and Environmental Engineering
and Geodetic Science
The Ohio State University

April 18, 2000

*PET On-Site CWO Lead Scientist, ERDC MSRC
†Senior Research Associate - Engineer

A Comparison of the SWAN and WAM Wave Models for Nearshore Wave Prediction

Abstract

A simulation of wind-wave activity during 1995 Hurricane Luis has been performed using the WAM and SWAN models. The WAM/SWAN interface option present in the SWAN code permits SWAN to be used as the finest nest of a nested WAM simulation. The purpose of this study was to test the WAM/SWAN interface option in SWAN Version 40.01 to determine whether SWAN could predict nearshore wave conditions more accurately than WAM. SWAN contains formulations for two physical processes not represented in the WAM code: depth-induced wave breaking and triad wave-wave interaction. Runs were made with and without these processes to determine their effects. Triad wave-wave interaction slightly improved the SWAN predictions for the test case used in this study. In contrast, depth-induced wave breaking noticeably improved the accuracy of the significant wave height predictions at the peak of the storm.

Keywords: WAM, SWAN, nearshore wave prediction, 1995 Hurricane Luis, depth-induced wave breaking.

1 Introduction

One of the major challenges in ocean modeling is the accurate prediction of nearshore wave conditions. Accurate nearshore wave conditions are necessary for environmental impact studies of erosion and sediment transport and play an equally important role in naval amphibious operations.

WAM (acronym for WAve Model) and SWAN (acronym for Simulating WAves Nearshore) are third-generation wave models used to compute random short-crested wind-generated waves on Eulerian grids. The WAM code has been primarily developed to generate open-ocean wave predictions necessary for naval operations and commercial ship movement, whereas SWAN has been developed and validated specifically in coastal and inland waters. Deep-water ocean waves are primarily wind-driven, but in nearshore zones, finite-depth effects such as bottom friction, shoaling, refraction, depth-induced breaking, and modified wave-wave interaction become important. In deep-water, quadruplet wave-wave interactions dominate the wave spectrum evolution , whereas in shallow water, triad wave-wave interactions become dominant. Thus, wave models like WAM, which only account for quadruplet wave-wave interaction processes, and do not account for depth-induced wave-breaking, may not predict coastal wave conditions as accurately as codes developed specifically for nearshore use.

The SWAN model includes a WAM/SWAN interface option which allows the boundary conditions for a fine-nest SWAN simulation to be provided by a coarse-nest WAM simulation. The boundary conditions are passed in the form of nonstationary energy-spectra in frequency-direction space. The aims of this study were to test the WAM/SWAN interface and to evaluate the nearshore wave predictions of the WAM and SWAN models. The selected test case is a three-nest simulation of wind-wave activity during 1995 Hurricane Luis for which NOAA buoy data were available as well as data from the U. S. Army Field Research Facility at Duck, NC. Comparison of the WAM and SWAN results with the wave observations permit evaluation of the two codes and may indicate areas where the models need to be improved.

A similar study was performed by Padilla et al. [7] for a severe North Sea storm which occurred in February 1993. In that study, two WAM nested grids were employed. The coarse mesh size contained 25x48 points with a cell size of 50 km and the fine nest contained 251x241 points with a cell size of 10 km. To compare the WAM and SWAN results, both codes were run on a Cartesian grid, depth-induced breaking and triad wave-wave interaction were not included. The studies differ in several aspects: 1) In the present study, the resolution cell size is approximately 2 km; 2) The WAM simulation was performed on a spherical grid while the SWAN was performed on a Cartesian mesh, thus, some minor differences can be expected and, 3) In the present study, SWAN included effects due to depth-induced wave breaking and triad wave-wave interactions. Runs were made with and without these processes activated to evaluate their effects.

2 Description of the SWAN and WAM codes

Although WAM and SWAN are both third generation wave models which compute random short-crested wind-generated waves, WAM was primarily developed for deep-water ocean waves, whereas SWAN has been developed specifically for coastal and inland waters. Both codes can be used for shallow and deep-water calculations and can include unsteady current and depth fields. The following basic physics are accounted for in both codes:

- Wave propagation in time and space
- Wave generation by wind
- Shoaling and refraction due to current and depth
- Whitecapping and bottom friction
- Quadruplet wave-wave interactions

The SWAN code contains formulations for two physical processes not present in the WAM code which can play an important role for nearshore calculations; they are a depth-induced wave-breaking

and triad wave-wave interaction. SWAN solves the spectral action balance equation

$$\frac{\partial}{\partial t}N + \frac{\partial}{\partial x}(c_x N) + \frac{\partial}{\partial y}(c_y N) + \frac{\partial}{\partial \sigma}(c_\sigma N) + \frac{\partial}{\partial \theta}(c_\theta N) = S/\sigma \tag{1}$$

where

$$S = S_{in} + S_{nl} + S_{wc} + S_{bf} + S_{dib} \tag{2}$$

and

$N(\sigma\theta)$ wave action density spectrum

σ the relative frequency

θ is the wave direction

S_{in} wind input

S_{nl} non-linear wave-wave interaction

S_{wc} dissipation due to whitecapping

S_{bf} dissipation due to bottom friction

S_{dib} depth-induced breaking

c_x, c_y propagation velocities in geographical space.

SWAN uses the wave action density spectrum, $N(\sigma\theta)$, rather than the energy density spectrum, $E(\sigma\theta)$, since in the presence of currents, the wave action density spectrum is conserved whereas the energy density spectrum is not. They are related through the relation

$$N(\sigma\theta) = E(\sigma\theta)/\sigma \tag{3}$$

SWAN solves the action balance equation on a Cartesian mesh using a fully implicit upwind scheme in geographical space. In directional and frequency space, the level of accuracy and diffusion can be selected by the user. The implicit scheme used in geographical space is unconditionally stable and thus avoids numerical instabilities. The implicit scheme allows the user the possibility to refine

the spatial mesh size to capture small scale effects without the necessity to reduce the time step to maintain stability. The details of the SWAN code are given by Booij et al. [1] and Ris et al. [2]. The SWAN code gives the user the option to select from different implemented physicals models, for example, there are three models for whitecapping and three for bottom friction. The different physical models can be found in the SWAN USER MANUAL [3] which can be downloaded from the SWAN web site (http://www.swan.ct.tudelft.nl). In this study, the source terms corresponding to those in WAM Cycle 4 were used (this is an option in the SWAN code).

The most recent release of the SWAN code (version 40.01) contains a number of improved features. Version 40.01 has a more accurate numerical estimation of the breaking of waves in the surf zone and the limiter used to stablize the quadruplet wave-wave interactions has been modified to avoid the undue damping of triad wave-wave interactions exhibited in earlier versions of the code. Model improvements have also been made for the case of very strong refraction. The most significant upgrade in version 40.01, is the option to use nonstationary boundary conditions. A restart capability has also been implemented, and stationary and nonstationary computations can be made in the same run.

The WAM model, described in Hassleman et al. [4], solves the wave-action transport equation

$$\frac{dE}{dt} + \frac{\partial}{\partial\phi}(\dot{\phi}E) + \frac{\partial}{\partial\lambda}(\dot{\lambda}E) + \frac{\partial}{\partial\theta}(\dot{\theta}E) + \frac{\partial}{\partial\sigma}(\dot{\sigma}E) = S_{in} + S_{wc} + S_{nl} + S_{bf} \tag{4}$$

where

- E represents the spectral density with respect to $(f, \theta, \phi, \lambda)$
- σ denotes frequencies
- θ directions
- ϕ latitudes
- λ longititudes

$\dot{\phi}$, $\dot{\lambda}$, and $\dot{\theta}$ are the rate of change of the position and propagation direction of a traveling wave

packet. The source terms are a superposition of the wind input, S_{in}, dissipation due to whitecapping, S_{wc}, bottom friction effects, S_{bf}, and nonlinear transfer processes S_{nl}.

WAM uses an explicit first-order accurate upwind scheme in geographical space and can propagate the solution on a Cartesian mesh or a spherical grid. A consequence of the explicit scheme is that the time step is proportional to the spatial step size, hence, as the mesh is refined the time step must be reduced to maintain stability, thus increasing the computational effort. WAM is one of the most extensively tested wave models in the world and is well documented. A detailed description of the WAM code is given by Gunther et al. [5] and Komen et al. [6].

Buoy locations

The SWAN and WAM computations were compared with the data from two NOAA buoys and the U. S. Army Field Research Facility 8 meters array (FRF 8M) and wave rider buoy 630 (FRF WR630) located at Duck, NC. These sites were selected since data was available for the 1995 September test period. The test locations and bathymetry are shown in Figure 1 where the Chesapeake Bay is indicated as "C. Bay" and the Albemarle Sound as "A. Sound." Water depths contours are shown. It can be seen from Figure 1 that NOAA buoy 44014 is situated in a water depth of 47.5 meters. The buoy is on the edge of the continental shelf. Beyond the shelf, the water depth increases rapidly to 3000 m. Table 1 summarizes the types of measurements available at the NOAA buoys and the FRF test sites with the notations for significant wave height (Hsig), peak wave period (Pper), and mean wave direction (Mdir).

Evaluation parameters

The computational results from the WAM and SWAN runs were examined based on the difference between the calculated values and the instrument measurements using root-mean-square (rms)

Table 1 Buoy location and water depths

Instrument ID	location	Water depth	Hsig	Mdir	Pper
NOAA buoy 44014	Virginia Beach, VA	47.5 m	yes	yes	yes
NOAA CHLV2	Chesapeake Light, VA	18.0 m	yes	no	yes
FRF WR630	Duck, NC	17.0 m	yes	no	yes
FRF 8m array	Duck, NC	7.0 m	yes	yes	yes

norms. The bias in the computations relative to the instrument measurements was also examined. These were computed using the ratios ΔH defined as:

$$\Delta H = \frac{H_c - H_b}{H_b} \tag{5}$$

where H takes on the values of significant wave height, mean wave period, and the mean wave direction and the subscripts "c" and "b" denote "computed" and "data" values. The root-mean-square norm (rms) and the bias are defined as:

$$rms(H) = \sqrt{\frac{1}{I}\sum_{i=1}^{I}(\Delta H_i)^2} \tag{6}$$

$$bias(H) = \frac{1}{I}\sum_{i=1}^{I}\Delta H_i \tag{7}$$

where "I" is the number of evaluation points.

Model deployments

The simulation period for this study was 08/29/95, 0 UTC to 09/13/95, 0 UTC. The evaluation period was taken as the 10-day period from 09/03/95, 0 UTC to 09/13/95, 0 UTC; the model spin-up portion of the simulation was not, therefore, used for evaluation purposes. The approximate path of the eye of Hurricane Luis from 08/29/95, 0 UTC to 09/10/95, 0 UTC is indicated by the

Figure 1 Bathymetry and Location of buoys

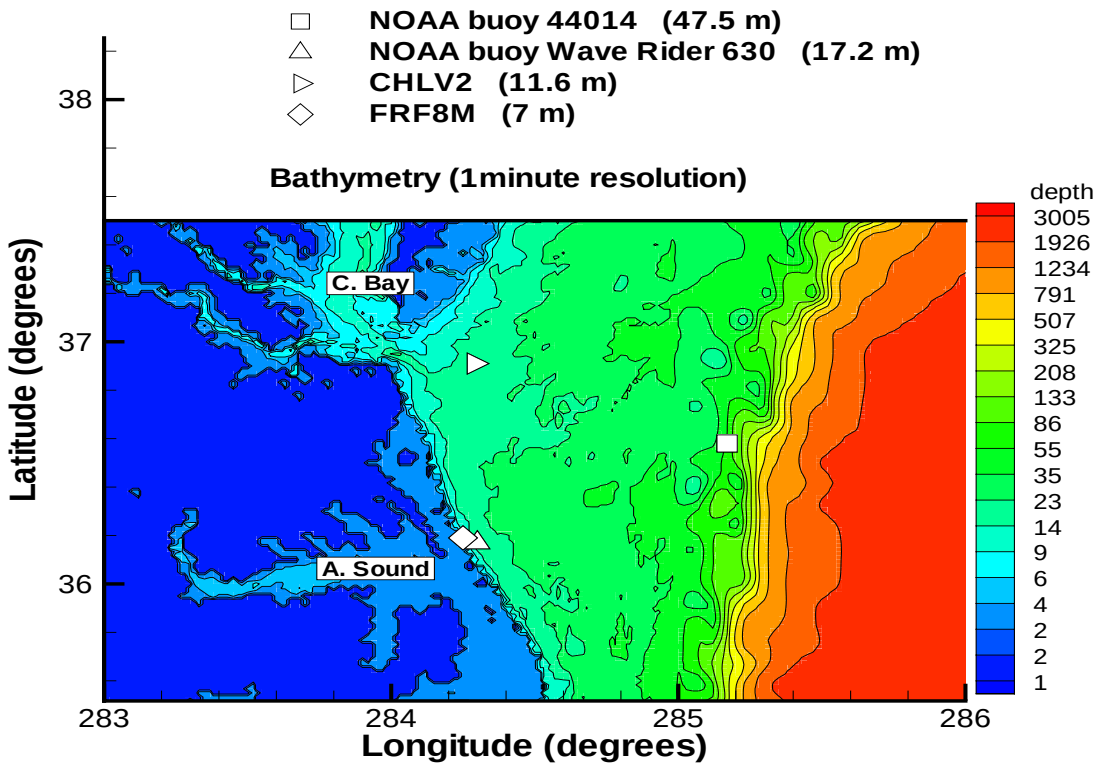

curving white line in Figure 2. The hurricane exhibited sustained winds up to 35 m/s and generated significant wave heights up to 4 meters at NOAA buoy 44014.

Although WAM and SWAN both use first-order time differencing, the implicit scheme in SWAN is more dissipative than the explicit scheme in WAM. This is true even if both codes are run using the limiting explicit time step. This can be shown by applying both the explicit and implicit schemes to the linear wave advection equation,

$$u_t + a u_x = 0 \;\; ; \;\; a > 0 \, . \tag{8}$$

It can be show that, (Tannehill et al. [10], for example), the modified equation being solved following discretization is

$$u_t + a u_x = \nu u_{xx} \ , \tag{9}$$

where the dissipation coefficients, ν, used later are given by

$$\nu_{exp} = a(1-\lambda)\Delta x_{exp}/2 \ , \tag{10}$$

and

$$\nu_{imp} = a(1+\lambda)\Delta x_{exp}/2 \ , \tag{11}$$

where λ is the Courant-Fredrichs-Levy (CFL) number, defined by

$$\lambda = \frac{a\Delta t}{\Delta x} \ . \tag{12}$$

A Von Neumann stability analysis leads to the condition $\lambda_{exp} \leq 1$; for the implicit case there is no restriction on the time step. Suppose we use the explicit limit for both schemes and take the component of the spectrum for which $\lambda = 1$. For the explicit scheme, this component of the spectrum travels undamped ($\nu_{exp} = 0$), whereas for the implicit scheme, it is damped by the coefficient $\nu_{imp} = a\Delta x$. Examining another component, for which $\lambda = 1/2$, the dissipative coefficients become

$$\nu_{exp} = a\Delta x/4 \ , \tag{13}$$

and

$$\nu_{imp} = 3a\Delta x/4 \ , \tag{14}$$

or

$$\nu_{imp} = 3\nu_{exp} \ . \tag{15}$$

Figure 2 Basin wind field : 09/10/95

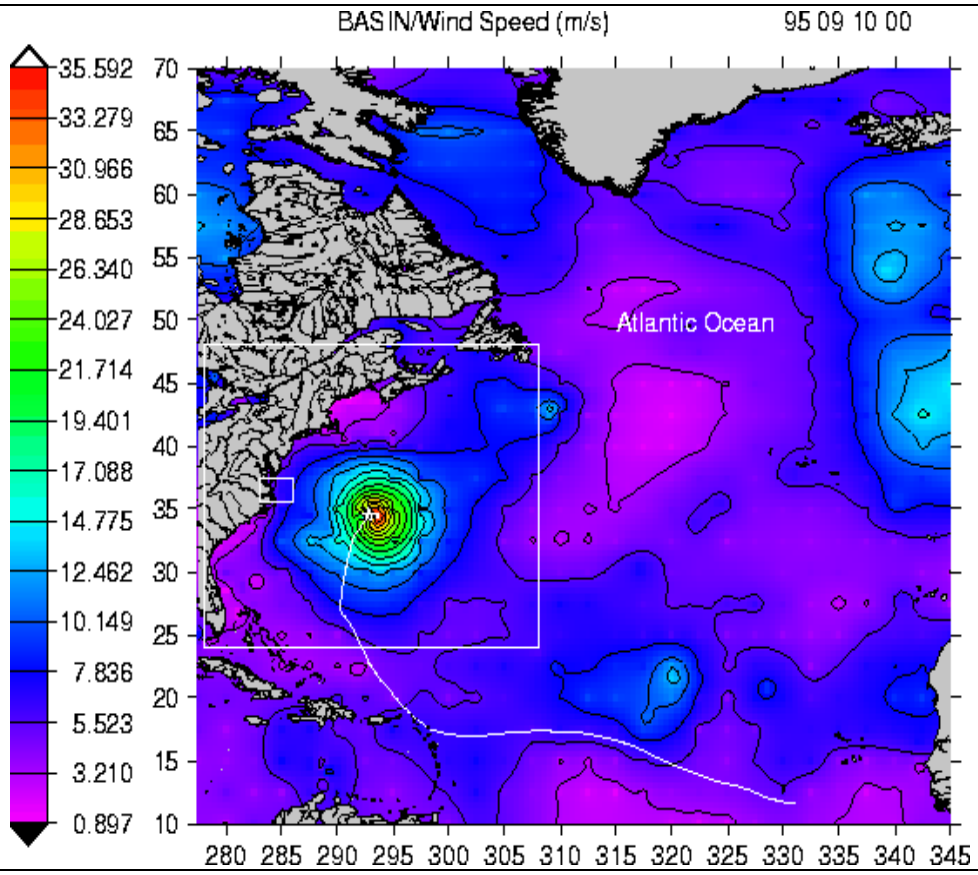

The implicit SWAN scheme is, therefore, always more dissipative than the explicit WAM scheme. For this reason, mesh refinement effects were examined for the SWAN code. It should be noted that the dissipative term becomes large where there are wave peaks (large curvature); these occur at the storm surges (peak of the storm). The dissipation coefficient is proportional to Δx, so as the mesh is refined, the dissipation coefficient becomes smaller.

The WAM calculations were performed on three nests, the nests are referred to as the "basin" (30-minute resolution; 135x121 cells), "region" (15-minute resolution; 120x96 cells), and the "sub-region" (5-minute mesh resolution; 36x24 cells), moving from coarser to finer resolution. Grid effects were examined for the sub-region using in addition to the 5-minute mesh resolution, a 5/2 minute resolution (72x48 cells) and a (5/4 minute resolution (144x96 cells). The three nests used in this study are shown in Figure 2. The results using the 144x96 mesh are presented here.

SWAN runs were made using sub-region meshes with 36x24, 72x48, and 144x96 cells; the two refined meshes reduce the implicit dissipative coefficient by 1/2 and 1/4 relative to the 36x24 mesh. Differences were noted in particular at the FRF8M test site where a large surge in the wave energy occurs at the height of the storm. The SWAN sub-region mesh with 144x96 cells was used for all of the results presented here.

Cardone wind fields [8] were used to drive the WAM and SWAN computations. The wind fields are defined on the basin nest. Bi-linear interpolation was used to obtain wind fields for the region and sub-region nests.

The three grid nests used in this study are shown in Figure 2. The figure shows a contour plot of the basin wind speeds at 09/10/95, 0 UTC, which approximately corresponds to the peak of the storm. At the top right of Figure 2 is the date and hour of the wind speed field shown. The state of Florida can be recognized in the lower left corner of the region nest. During the basin computation, predicted wave spectra are interpolated to the boundaries of the region and saved. Likewise, during the computations for the region, spectra are interpolated to the boundaries of the sub-region and saved. The boundary condition spectra, the winds, and the bathymetry drive the computations for the different nests.

The coordinates used to plot the hurricane eye path in Figure 2 were obtained from the NOAA National Buoy Center web site and are not taken from the Cardone wind fields. Overlaying the NOAA data on contour plots of the Cardone wind speeds served to validate that the Cardone wind speeds were consistent with the NOAA data. Figure 3 shows the WAM significant wave height for the region at 0 UTC, September 10th which corresponds to the wind speeds shown in Figure 2. The sub-region is the white box in Figure 3. Figure 4 shows the SWAN significant wave height contours for the sub-region for the same date. The contour lines in the lower right of Figure 4 are smooth as the deep-water bathymetry does not affect the waves. As the waves approach the nearshore zone, the contours show the dissipation of wave energy at shallow depths.

Table 2 shows pertinent information regarding the WAM runs. For both the WAM and SWAN

Figure 3 Region significant wave height: 09/10/95, 0 UTC

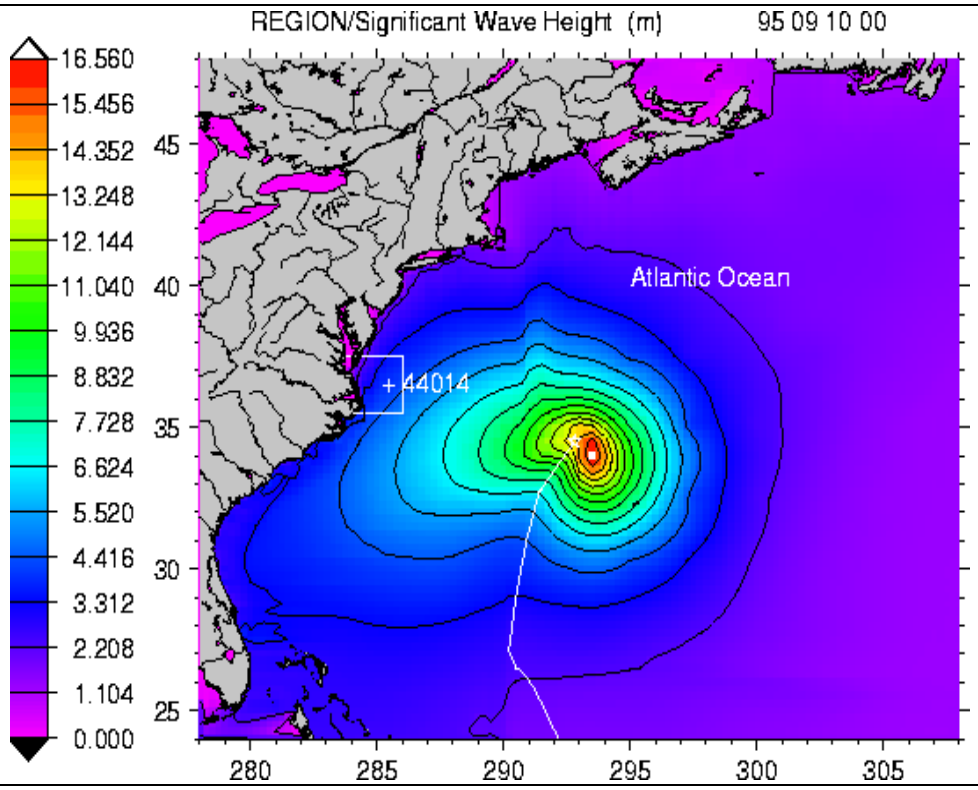

calculations, 25 frequencies and 24 directions were used with the lowest frequency being 1/30 Hertz. The WAM grids were spherical and generated from the latitude and longitude found in Table 2. The bathymetry data was supplied by Dr. Robert Jensen of the U. S. Army Engineer Research and Development Center. SWAN requires the grid point locations to be defined in meters, along with the longititude and latitude of the southwest corner point. The SWAN grid node spacings were generated using the equations

$$\Delta latitude_m = F * \Delta latitude_d \, , \tag{16}$$

and

$$\Delta longitude_m = F * \Delta longitude_d * \beta \, , \tag{17}$$

Figure 4 Swan significant wave height: 09/10/95, 0 UTC

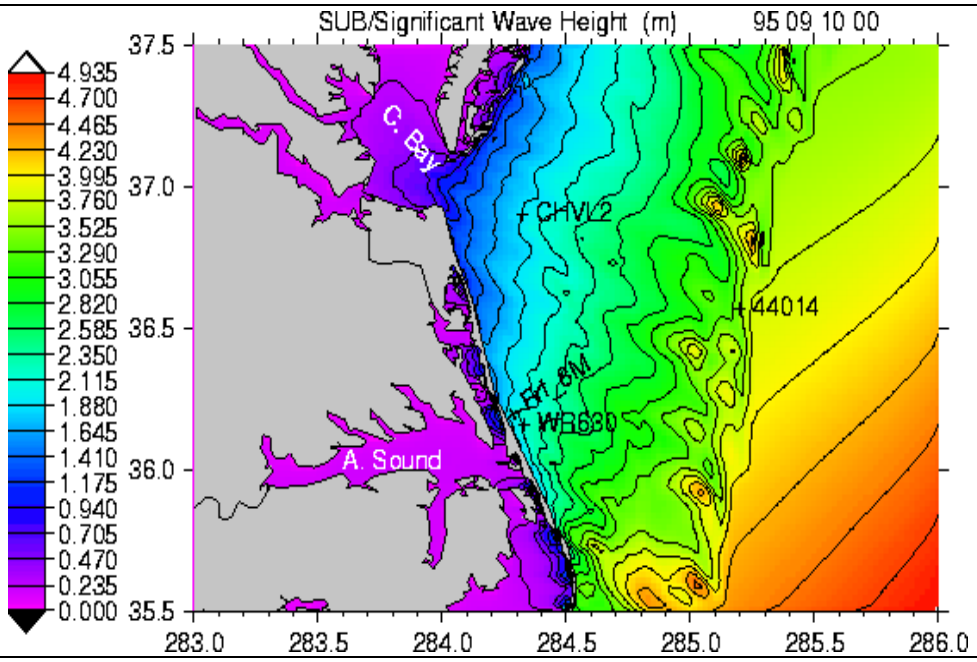

where

$$\beta = cos(\frac{\pi}{180} * latitude_d) \ , \tag{18}$$

and

$$F = \frac{Earth's\ circumference\ at\ the\ Equator\ (meters)}{360} \ , \tag{19}$$

where the subscripts "m" and "d" denote meters and degrees, respectively. The Earth's circumference at the Equator was taken as 40,000,000 meters. The factor β accounts for the variation with latitude of the length (in meters) of a fixed increment (in degrees) due to the Earth's curvature.

Table 3 shows the water depths for both the WAM and SWAN codes on the 144x96 mesh. The depths for WAM were obtained by bi-linear interpolation.

Table 2 WAM data

Description	basin	region	sub-region 1	sub-region 2	sub-region 3
max/min longitude	345/277.5	308/278	286/283	286/283	286/283
max/min latitude	70/10	48/24	37.5/35.5	37.5/35.5	37.5/35.5
cell size (min)	30 min	15 min	5 min	5/2 min	5/4 min
cell size (deg)	1/2	1/4	1/12	1/24	1/48
cell size (km)	56	28	9	4.6	2.3
number of cells	135x129	120x96	36x24	72x48	144x96
Propagation time step	12 min	6 min	2 min	2 min	1 min
Source time step	12 min	6 min	2 min	2 min	1 min

Table 3 Simulation buoy location and water depths

Instrument ID	location	test site	WAM	SWAN
NOAA buoy 44014	Virginia Beach, VA	47.5 m	57	31
NOAA CHLV2	Chesapeake Light, VA	18.0 m	17	17
FRF WR630	Duck, NC	17.0 m	17	12
FRF 8m array	Duck, NC	7.0 m	3	4

3 Discussion of results

The SWAN results shown in Figures 5-14 were obtained with quadruplet wave-wave interaction and depth-induced wave-breaking switched on, but with triad wave-wave interaction switched off. SWAN simulations were run for integration time steps of 2 and 12 minutes. The differences were small and the 12 minute time-step was used for the calculations presented here.

Results for NOAA buoy 44014

Figures 5-7 show comparisons between the computed significant wave heights, mean wave direc-

tions, and peak wave periods and the NOAA buoy 44014 measurements over the 10-day evaluation period. It should be noted that the wave direction convention used in this paper is the direction waves are coming from, in terms of the compass standard. Also shown in the figures are the rms error and bias values. In these figures, WAM and SWAN show similar levels of accuracy with the exception of peak wave period, where SWAN is more accurate. The time phase behavior for significant wave height is approximately the same for both codes and the peak wave period is predicted equally well by both codes.

Figure 5 Time series of significant wave height: NOAA buoy 44014

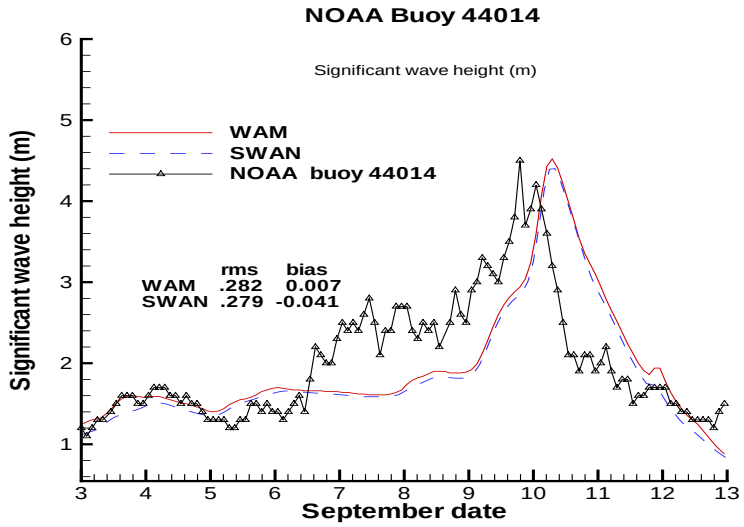

As NOAA buoy 44014 is situated in a water depth of 47.5 meters, deep-water effects are dominant; depth-induced wave breaking should not play a role and the two codes should produce similar results. The slight differences may be due to the differences in the numerical algorithms used in geographical space, different model parameters, and the different mesh types (WAM spherical grid versus SWAN Cartesian grid).

Figure 8 shows the Hsig/depth ratios at the different test sites computed from the buoy measurements. The ratios are small ($\approx .08$) at buoy 44014, confirming deep-water wave behavior. We note that the term "nearshore" is not a precise term. The ratio Hsig/depth can, however, be used to indi-

Figure 6 Time series of mean wave direction: NOAA buoy 44014

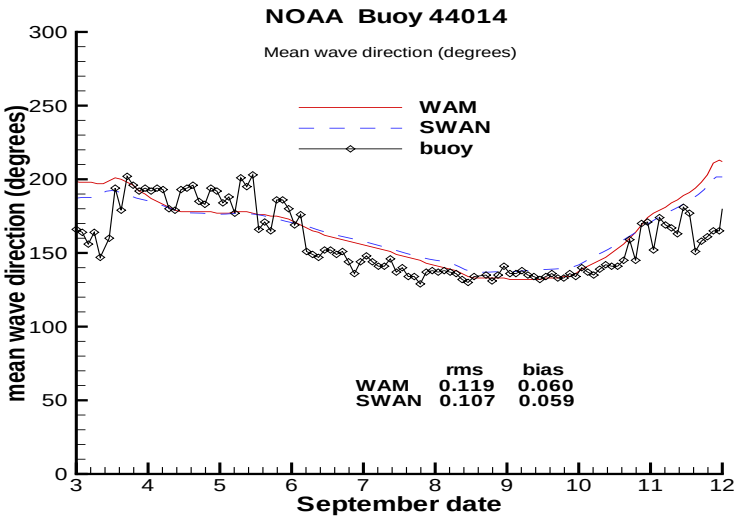

cate the importance of depth-induced breaking and the type of wave-wave interactions (quadruplet or triad) which are dominant.

Results for NOAA buoy CHLV2

Figures 9-10 show comparisons between the computed significant wave heights and peak wave period and the buoy measurements. In Figure 9, WAM and SWAN show similar trends for the significant wave height, with both codes greatly overpredicting the significant wave height at the peak of the storm. Figure 10 shows that the peak wave period is predicted equally well by both codes. At the peak of the storm, the Hsig/depth ration is $\approx .16$.

Results for NOAA buoy WR630

Figures 11-12 show comparisons between the computed significant wave heights and peak wave periods and the buoy measurements. In Figure 11, the two models' significant wave heights are approximately the same until the peak of the storm. Figure 12 shows that the peak wave period is

Figure 7 Time series of peak wave period: NOAA buoy 44014

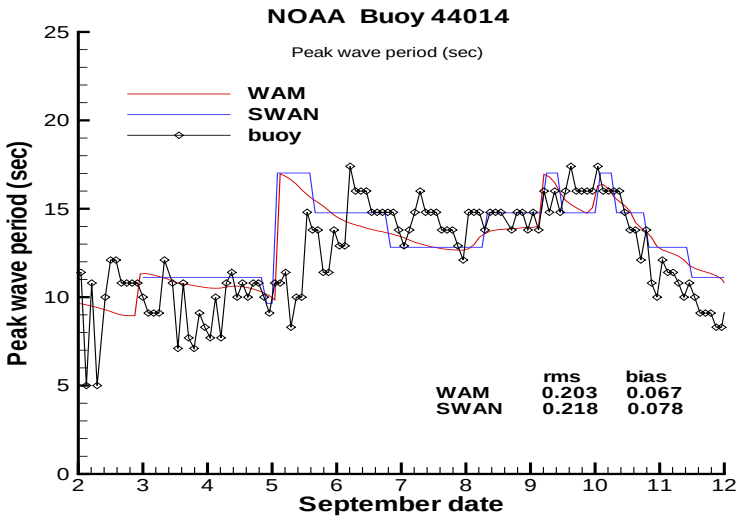

predicted equally well by both codes. The ratio of Hsig/depth is ≈ 0.15 at the peak of the storm.

Results for FRF 8 meter array

Figures 13-14 show comparisons of the computed significant wave heights and peak wave periods and the instrument measurements. Figure 13 shows that WAM is more accurate except at the peak of the storm where SWAN is more accurate. This behaviour can also be seen to a lesser extent in Figures 9 and 11. Figures 14-15 show SWAN and WAM predicting the mean wave direction and the peak wave period equally well.

Depth-induced wave-breaking

The notable differences between the WAM and SWAN predictions of significant wave height at FRF8M at the peak of the storm, were initially thought to be due to the coarse nature of the sub-region mesh first used in WAM ("sub-region 1" in Table 2; 36x24 cells). It was supposed that the coarse bathymetry resolution had caused inaccurate prediction of depth-related effects. To clarify this issue, two additional WAM sub-region runs were made using a 72x48 cell mesh ("sub-region 2" in Table 2), and a 144x96 cell mesh ("sub-region 3" in Table 2) but this bathymetry refinement

Figure 8 The Hsig/depth ratios at test sites

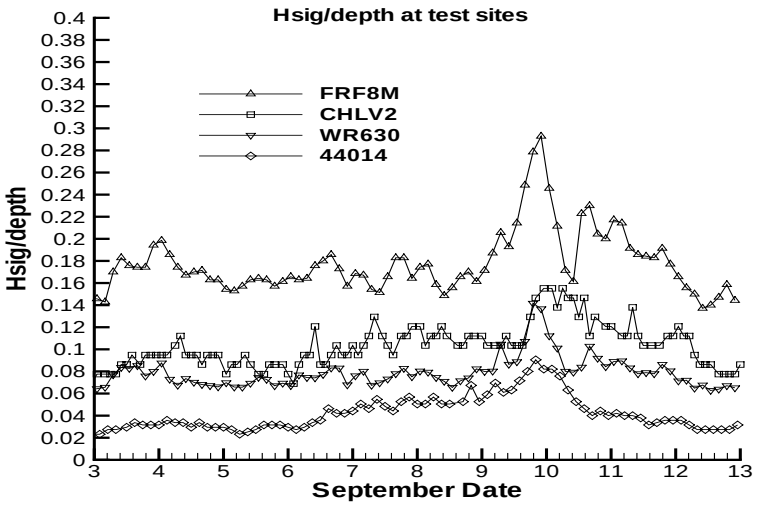

only led to small differences. A second SWAN run was next performed with the depth-induced wave breaking process switched off in order to evaluate its impact. Depth-induced breaking in SWAN is accounted for by using the random-bore model of Battjes and Jansen [9], with improvements by Nelson [11]; WAM does not have a depth-induced breaking formulation. Figure 16 shows the SWAN wave height predictions with and without wave breaking. It can be seen that the SWAN solution is much closer to the WAM solution when depth-induced breaking is switched off. At the peak of the storm the ratio Hsig/depth becomes large (0.20) and wave-breaking clearly becomes important at FRF8M. At the other test locations, the SWAN wave-breaking model had negligible impact; this was also the case for the wave direction at the FRF8M site.

Quadruplet and triad wave-wave interactions

Figure 17 shows a comparison between the SWAN results at the FRF8M test site obtained with only the quadruplet wave-wave interaction formulation and the results obtained accounting for both quadruplet wave-wave and triad wave-wave interactions. It can be seen that the inclusion of triad wave-wave interactions slightly improves accuracy. It is clear, however, that at the peak of

Figure 9 Time series of significant wave height: NOAA CHLV2 buoy

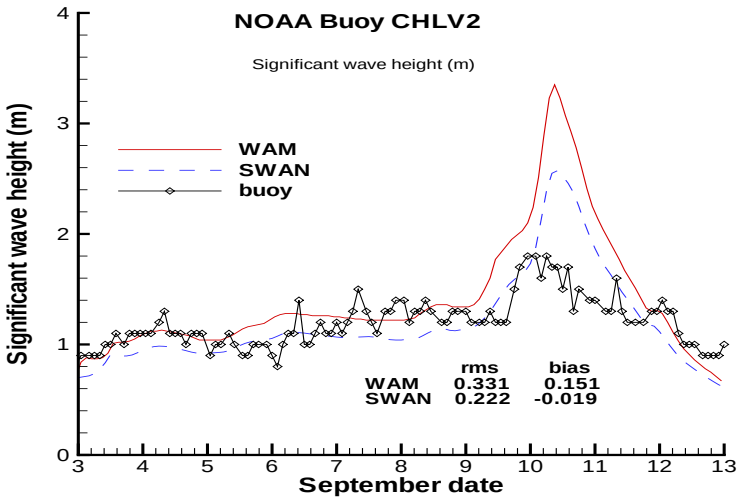

the storm, depth-induced wave-breaking becomes a dominant process in the shallow water region around FRF8M.

Summary

The WAM/SWAN wave model boundary condition interface option present in the SWAN Version 40.01 code has been tested and WAM and SWAN predictions have been compared with measurements at four test sites. The selected test case was a simulation of wave activity during 1995 Hurricane Luis for which NOAA buoy data was available as well as data from the U. S. Army Field Research Facility at Duck, NC. A three-nest simulation was performed, making WAM runs on all three nests and SWAN runs on the finest nest using boundary conditions from WAM. The purpose of this study was to determine whether SWAN, a model developed specifically for coastal and inland waters, could predict nearshore wave conditions more accurately than WAM. A summary of the model evaluation statistics is given in Table 4. The statistics show a small accuracy bias towards SWAN for seven of the ten comparisons. The accuracy bias and small rms errors indicate that one can have confidence in applying the SWAN code to shallow water regions and making use of the WAM/SWAN interface

Figure 10 Time series of mean wave direction: NOAA CHLV2 buoy

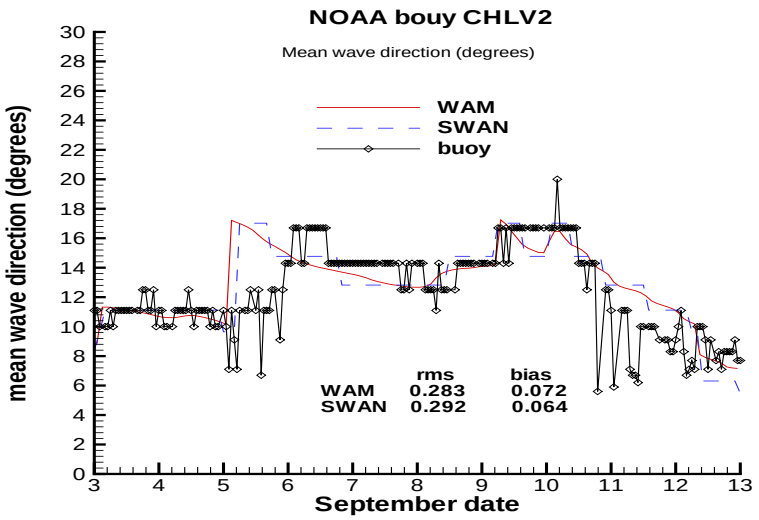

to supply boundary conditions.

In conclusion, the results show:

• In general, SWAN and WAM predict equally well the peak wave period.

• In regions where the Hsig/depth ratio becomes large, (for example, at the FRF8M test site at the peak of Hurricane Luis), SWAN clearly predicts the significant wave height more accurately than WAM. The improved accuracy results from the inclusion of the depth-induced wave-breaking process present in the SWAN code.

• SWAN runs made accounting for quadruplet wave-wave interactions and both the quadruplet and triad wave-wave interaction showed that accounting for triad wave-wave interactions slightly improved the wave predictions at the FRF8M test site.

4 Acknowledgement

This work was supported in part by a grant of HPC time from the DoD HPC Modernization Program. The authors would like to thank Dr. Robert Jensen of the Coastal and Hydraulics Laboratory at the U. S. Army Engineer Research and Development Center for suggesting and supporting this

Table 4 Comparison of RMS errors

	significant wave height		
buoy	WAM	SWAN	accuracy bias
NOAA 44014	0.282	0.279	SWAN
NOAA CHLV2	0.331	0.222	SWAN
FRF WR630	0.373	0.261	SWAN
FRF 8 meter	0.494	0.255	SWAN
	peak wave period		
NOAA 44014	0.203	0.218	WAM
NOAA CHLV2	0.283	0.292	WAM
FRF WR630	0.251	0.243	SWAN
FRF 8 meter	0.202	0.203	WAM
	mean wave direction		
NOAA 44014	0.119	0.107	SWAN
FRF 8 meter	0.133	0.107	SWAN

study, providing the Hurricane Luis wind fields and making possible the visit of Professor IJsbrand Haagsma of the SWAN development team. The help and many fruitful discussions with Professor IJsbrand Haagsma during his visit are greatfully acknowledged. The first author would like to thank the other members of the SWAN support team at the Delft University of Technology in the Netherlands for their help. The many discussions with Erick Rogers of Planning Systems, Inc. concerning the SWAN code were greatly appreciated.

Figure 11 Time series of significant wave height: NOAA WR630 buoy

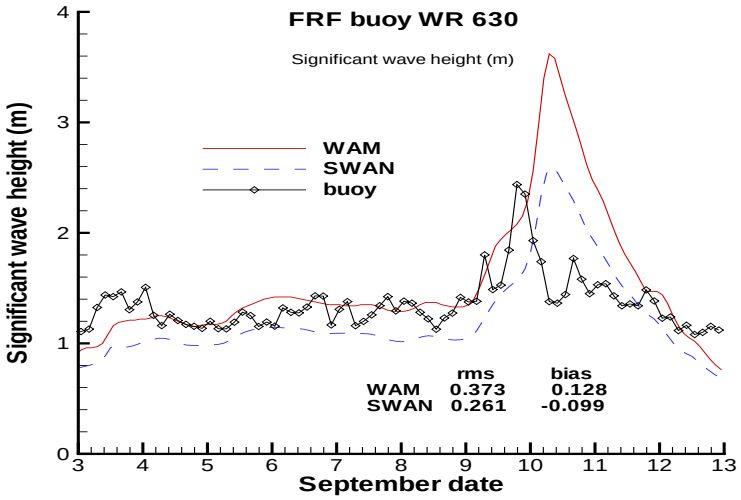

Figure 12 Time series of peak wave period: NOAA WR630 buoy

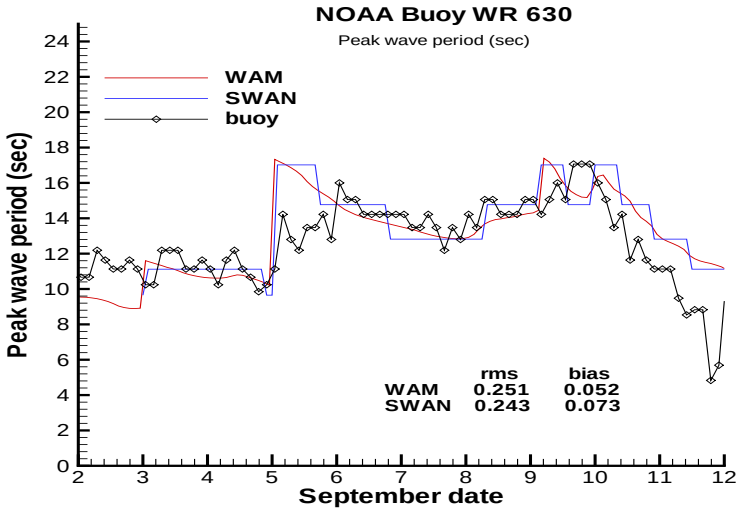

Figure 13 Time series of significant wave height: FRF 8 meter array

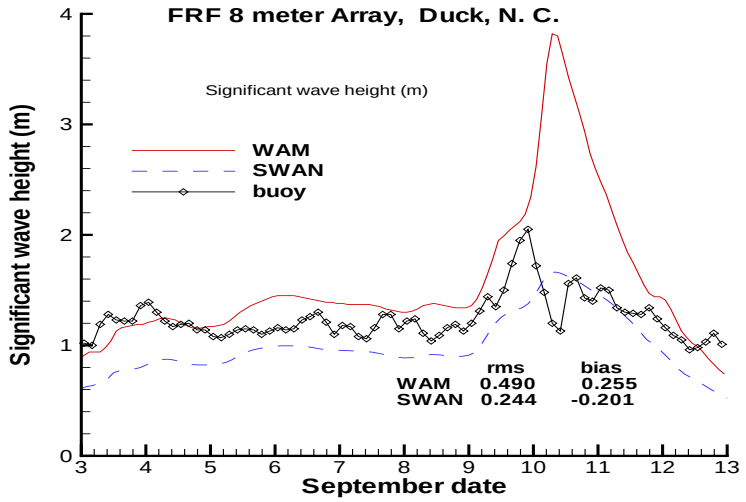

Figure 14 Time series of mean wave direction: FRF 8 meter array

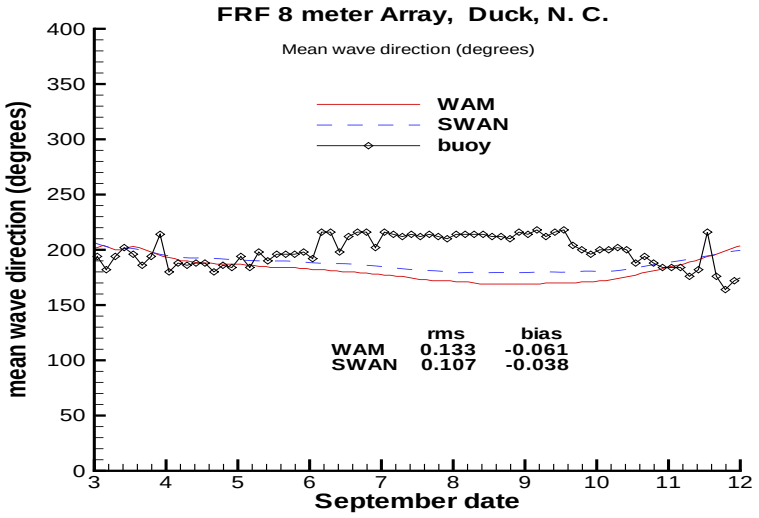

Figure 15 Time series of peak wave period: FRF 8 meter array

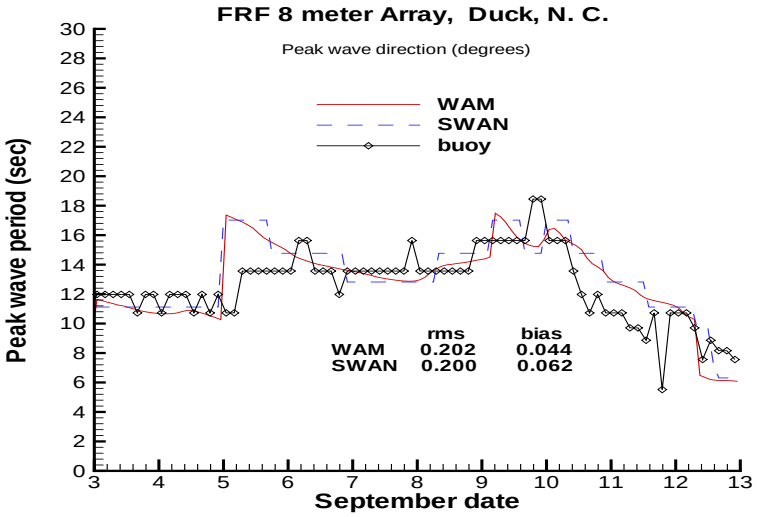

Figure 16 The effect of the SWAN depth-induced wave-breaking model: FRF 8 meter array

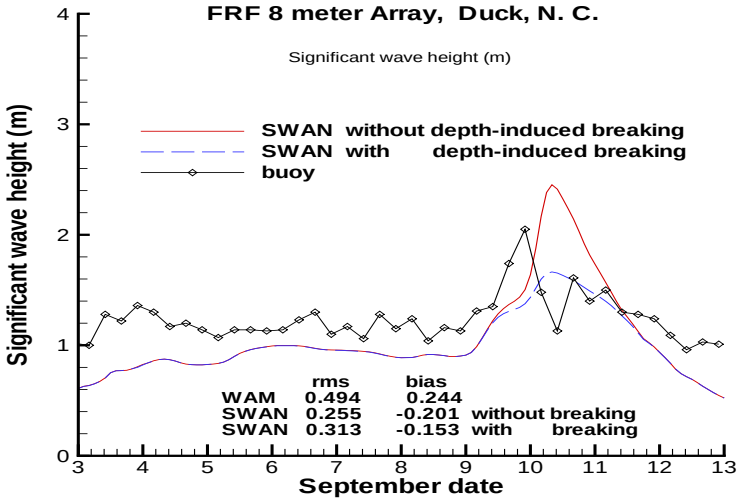

Figure 17 Quadruplet vs. triad wave-wave interaction

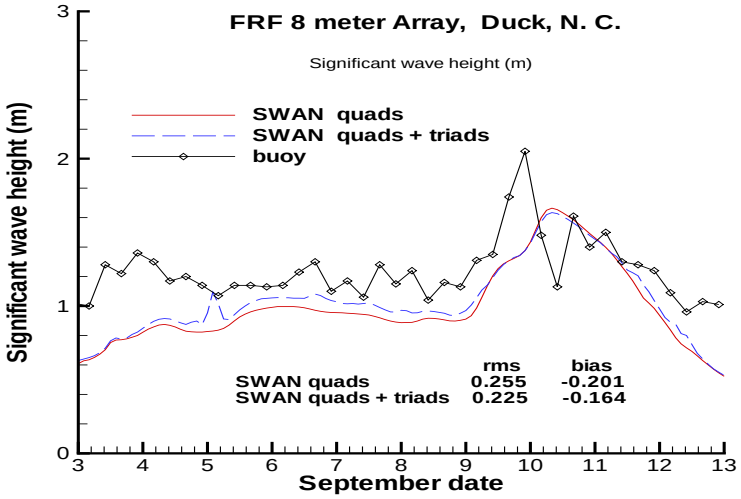

References

[1] Booij, N., Ris, R.C. and Holthuijsen, L. H., 1999, "A third-generation wave model for coastal regions, Part I, Model description and validation," *J. Geoph. Research* 104, C4, 7649-7666.

[2] Ris, R.C., Booij, N. and Holthuijsen, L. H., 1999 "A third-generation wave model for coastal regions, Part II, Verification," *J. Geoph. Research* 104, C4, 7667-7681.

[3] Holthuijsen, L. H., Booij, N., Ris, R.C., Haagsma, IJ. G., Kieftenburg, A.T.M.M., and Padilla-Hernandes, R.,"SWAN version 40.01 USER MANUAL." November 3, 1999

[4] Hasselmann, S., Hasselmann, K., Buer, E., Janssen, P. A. E. M., Komen, G.J., Bertotti, L., Lionello, P., Guillaume, A., Cardone, V. C., Greenwood, J. A., Reistad, M., Zambresky, L., and Ewing, J. A., 1988, "The WAM model - a third generation ocean wave prediction model," *J. Physical Oceanography*, 18, 1775-1810.

[5] Gunther, H. P., Hasselmann, K., Hasselmann S., and Janssen, P. A. E. M., 1992, "The WAM model Cycle 4," DKRZ Report No. 4, Hamburg.

[6] Komen, G.J., Cavaleri, L., Donelan, M., Hasselmann, K., Hasselmann, S., and Janssen, P. A. E. M., 1994, "Dynamics and Modelling of Ocean Waves," *Cambridge University Press*, Cambridge

[7] Padilla, R., Osuna, P., Monbaliu, J, and Holthuijsen, L., "Intercomparing third-generation wave model nesting," 5th International Workshop on Wave Hindcasting and Forecasting, Melbourne, Florida, January 26-30, 1998.

[8] Cox, A. T., Greenwood, J. A., Cardone, V. J., and Swail, V. R., 1995, "An Interactive Objective Kinematic Analysis System," 4th International Workshop on Wave Hindcasting and Forecasting, Banff, Alberta.

[9] Battjes, J. A. and Janssen, P. A. E. M., 1978, "Energy loss and set-up due to breaking of random waves" Proc. 16th Int. Conf. Coastal Engineering, ASCE, 569-587.

[10] Tannehill, J. C., Anderson, D. A. and Pletcher, R. H., 1997, Computational Fluid Mechanics and Heat Transfer, Second Edition, Taylor and Francis.

[11] Nelson, R. C., "Depth limited wave heights in very flat regions," *Coastal Engineering*, 23, 43-59, 1994.